A Methodological Framework for Prognosis Using Control-Oriented Models: Application to an Aeronautical Power Converter

MOHAMED SKAIK[1], LAURENT SAINTIS[1], SYLVAIN VERRON[1], and NICOLA ESPOSITO[2]

[1] *Univ Angers, LARIS, SFR MATHSTIC, F-49000 Angers, France*
mohamed.skaik@univ-angers.fr
laurent.saintis@univ-angers.fr
sylvain.verron@univ-angers.fr

[2] *University Scuola Superiore Meridionale, Napoli, Italy*
n.esposito@ssmeridionale.it

ABSTRACT

Developing Prognostics and Health Management (PHM) for safety-critical systems faces a major challenge. Obtaining degradation and failure data is both expensive and time-consuming, especially during the design and development phases. Models built at this stage for control specification and verification, such as those in MATLAB/Simulink using the Specialized Power Systems toolbox, were not designed to capture component faults or track degradation over multi-year aging horizons. In addition, their single-domain electrical focus neglects important multi-physics interactions like electro-thermal feedback. To address this gap, this work applies a parametric four-stage workflow that leverages the computational efficiency of electrical models, making long-duration degradation simulations practical for data generation. We apply this approach to an aeronautical power converter, with the Silicon Carbide (SiC) Metal-Oxide-Semiconductor Field-Effect Transistor (MOSFET) selected as the most reliability-critical component. The increase in on-state resistance is used as the principal degradation indicator. Without altering the model's structure, degradation is introduced through controlled parametric fault injection to generate structured degradation datasets, followed by systematic feature engineering of electrical signatures to identify degradation-sensitive patterns. Top-ranked features are then used to train regression models that provide a diagnostic estimate of fault severity. This end-to-end workflow validates the PHM pipeline using available design-stage tools, establishing a performance baseline and reducing technical risk before transitioning to higher-fidelity multi-physics co-simulation.

1. INTRODUCTION

In safety-critical aerospace systems, the ability to predict failures before they occur is essential, not just for safety, but for maintaining operational availability. This is especially important for power electronic converters, where components like Silicon Carbide (SiC) Metal-Oxide-Semiconductor Field-Effect Transistors (MOSFETs) gradually degrade over time [1]. As these devices age, their on-state resistance ($R_{\mathrm{DS(on)}}$) increases due to thermo-mechanical fatigue and gate-oxide degradation, leading to higher energy losses and thermal stress that can accelerate their decline. The resulting drift in $R_{\mathrm{DS(on)}}$ has therefore become one of the most widely used aging precursors in power MOSFET prognostics [1–3]. Building effective Prognostics and Health Management (PHM) during the design phase is challenging because the data needed to develop and validate predictive models, whether from aging tests or operational experience, is not yet available.

The Aeroconverter project exemplifies this challenge. This industry-academia collaboration, sponsored by Airbus, aims to develop a highly reliable power converter for pressurized aircraft environments where safety requirements are stringent. One critical measure is the Mean Time Between Unscheduled Removal (MTBUR), which drives the need to move from reactive maintenance to predictive strategies [4]. Developing PHM capabilities for the converter is therefore a project requirement, and the present work is an early step in that direction.

Existing approaches to PHM development for power electronic systems generally fall into three categories, each facing practical constraints at the design stage. Physics-of-failure (PoF) models provide high physical fidelity by linking material-level degradation mechanisms to component-level behavior, but require detailed thermal

characterization and material properties that are unavailable before hardware fabrication [5].
Electro-thermal co-simulation environments can capture the interactions between thermal stress and electrical degradation [6], but they also require thermal characterization data, such as package thermal impedances and material properties, that are not yet available at this stage of the project. Direct experimental aging campaigns yield the most realistic degradation trajectories [2, 7], but require physical hardware, specialized testing infrastructure, and timescales of months to years that are fundamentally incompatible with the design phase. As a result, PHM algorithm development is typically deferred until hardware is available, increasing technical risk and delaying validation at the stage when design changes are least costly.

The existing Specialized Power Systems (SPS) electrical model of the Aeroconverter was originally developed for control design and verification, not for PHM purposes. While it excels at validating electrical performance and control strategies under nominal conditions, it is purely electrical and does not explicitly model electro-thermal or thermo-mechanical degradation processes. However, it offers significantly faster simulation speeds compared to full multi-physics models. Retaining this model represents a deliberate trade-off: we gain rapid execution of large simulation ensembles, but accept that physical aging mechanisms and temperature fields are not explicitly represented.

This raises a practical question that is the central motivation of this work: can an existing control-oriented model, already present at the design stage for electrical verification, generate sufficiently informative degradation data to support algorithm development and instrumentation planning before hardware becomes available? The present work makes two contributions toward answering this question.

First, we demonstrate that a fast, single-domain electrical model can produce discriminative degradation signatures when systematically configured, generating a complete labeled dataset in hours rather than weeks. Second, by evaluating candidate features across all instrumented measurement points, the framework identifies which electrical signals carry the most prognostic and diagnostic information about MOSFET degradation, providing actionable guidance on instrumentation priorities before hardware layout is finalized. The accuracy achieved with existing design-stage tools confirms the feasibility of this approach and establishes a reference baseline for subsequent higher-fidelity modeling and experimental campaigns.

These contributions are pursued through the standard PHM pipeline of data acquisition, feature extraction, health assessment, and fault prediction [8], applied here to SiC MOSFET degradation in the aeronautical DC/DC converter.

The paper is structured as follows. Section 2 describes the system and failure physics. Section 3 details the methodology. Section 4 presents and discusses the results. Section 5 concludes with limitations and directions for future work.

2. SYSTEM MODELING & FAILURE PHYSICS

2.1. Aeronautical Power Converter and SPS Model

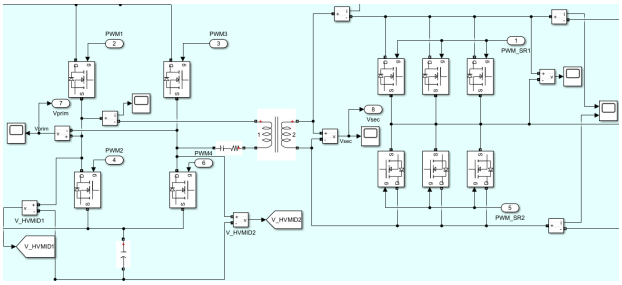

Figure 1. Power Stage of the PSFB Converter Model

The system under study is a 10 kW phase-shifted full-bridge (PSFB) DC/DC converter (Fig. 1) being developed within the Aeroconverter project, a DGAC-funded program supported by Airbus under ATA 24 (Electrical Power). Designed for installation in pressurized aircraft zones, the converter must satisfy stringent Development Assurance Level B (DAL-B) requirements [9] while providing galvanic isolation and stable low-voltage power to the onboard distribution network. It converts a high-voltage DC bus (440–620 V) to a regulated 28 V DC output, supplying the aircraft's low-voltage loads with high efficiency and controlled ripple. Because it is integrated into the primary electrical architecture, any unscheduled removal directly impacts aircraft availability and maintenance costs, making improved reliability and increased MTBUR a central objective.

In the current project phase, the converter is represented by an existing SPS electrical model [10] that uses idealized switching elements and lumped passive components, optimized for fast electromagnetic transient simulation of the closed-loop converter and its interaction with the electrical network.

2.2. Reliability-Critical Component: SiC Power Modules

The primary switching elements in the converter are SiC power modules, selected to meet the project's efficiency, power density, and thermal performance targets under demanding aeronautical operating conditions. As in other high-power converters, these modules are among the most vulnerable elements in the power path. Reliability studies consistently show that semiconductor devices account for a significant share of converter failures [11].

Degradation mechanisms such as bond-wire fatigue, solder-joint fatigue, and gate-oxide wear-out modify conduction and switching losses, disturb dynamic behavior, and can ultimately drive the converter outside its specified operating envelope [12]. Incipient damage at module level may therefore manifest as increased losses, altered current and voltage waveforms, and degraded regulation of the 28 V DC bus before any hard failure occurs. For these reasons, the SiC power modules are treated as the primary reliability-critical components and selected as the target of the prognostic framework.

2.3. Failure Precursor: On-State Resistance $R_{\text{DS(on)}}$

The progressive increase of the on-state drain-source resistance ($R_{\text{DS(on)}}$) of the SiC MOSFETs is used as the primary degradation variable in this work. Physically, $R_{\text{DS(on)}}$ aggregates the combined effects of multiple aging mechanisms acting at both die and package levels, including channel mobility degradation and bond-wire fatigue [11, 12]. Since these mechanisms manifest collectively as a measurable increase in $R_{\text{DS(on)}}$, this parameter serves as a macroscopic health index of the aggregate aging state of the device. Both Si and SiC power MOSFET prognostic studies consistently identify $R_{\text{DS(on)}}$ as a stable and repeatable precursor of impending failure [2, 3, 5].

$R_{\text{DS(on)}}$ responds to two distinct influences, and both raise its value. Device aging produces an irreversible increase, which is the quantity we use as the degradation signal. Junction temperature produces a reversible increase: $R_{\text{DS(on)}}$ rises as the device heats and returns toward its baseline once it cools. Any health indicator built on $R_{\text{DS(on)}}$ must therefore separate the slow irreversible drift from this faster reversible thermal modulation. We address this here by extracting features at a single fixed operating point, so the thermal contribution stays constant and the variation seen across runs is attributable to aging alone. Isolating the two contributions on real hardware, where temperature varies with load and ambient conditions, will require either measurement at a controlled reference temperature or a concurrent junction-temperature reading to compensate the thermal term before estimating k.

The degradation state is parameterized through a multiplicative scaling factor k applied to the nominal on-state resistance:

$$R_{\text{DS(on)},i} = R^{\text{nom}}_{\text{DS(on)}} \times k_i, \quad k_i \in \{1.00, 1.01, \ldots, 1.25\} \quad (1)$$

with $k = 1.00$ corresponding to the nominal healthy state and $k = 1.25$ to the conventional end-of-life threshold for power MOSFETs [11]. Each value of k represents a snapshot of the converter at a specific degradation state, independent of the temporal path that produced it: a device at $k = 1.10$ after 2,000 hours of high-stress operation is electrically indistinguishable from one reaching it after 8,000 hours of moderate use. This separates the characterization of degradation states from the temporal degradation law $k(t)$ governing how those states are reached.

3. METHODOLOGICAL FRAMEWORK

The methodology applied here follows four stages, each addressed in the subsections below.

3.1. Stage 1: Model Configuration and Optimization

The baseline configuration had serious scalability problems: each 70 ms simulation took roughly three hours of wall-clock time and generated over 2 GB of output data. Additionally, sensor signals were aggregated into a single logging bus rather than individually traceable channels.

To repurpose this model for prognostic data generation, three targeted changes were made to its configuration, leaving the underlying circuit model unchanged:

- **Sensor instrumentation:** The model's sensor configuration was aligned with the physical converter instrumentation plan to ensure that simulated observables correspond to physically measurable quantities on actual hardware. Table 1 defines the monitored signals and their measurement locations.
- **Signal logging reconfiguration:** Each sensor channel was configured to record individually at 500 kHz sampling rate, consistent with typical high-speed sensor capabilities in the hardware design, enabling per-signal feature extraction and traceability.

Table 1. Monitored Signals and Measurement Locations

Signal	Type	Measurement Location
High-Voltage Input Side		
V_{HV1}	Voltage	HV input connector
V_{HV2}	Voltage	Before H-bridge
I_{HV1}	Current	HV circuit input
V_{MID1}, V_{MID2}	Voltage	H-bridge midpoint
Low-Voltage Output Side		
V_{LV1}, V_{LV2}	Voltage	After transformer
V_{LV3}, V_{LV4}	Voltage	Before main contactor
V_{LV5}	Voltage	After main contactor
I_{LV1}	Current	Before filtering capacitor
I_{LV2}	Current	After filtering capacitor

- **Computational Efficiency Optimization:** The PSFB converter model is formulated as a system of ordinary differential equations (ODEs) derived from Kirchhoff's voltage and current laws applied to the switching network, with state variables representing inductor currents and capacitor voltages. PWM switching at

100 kHz introduces rapid state transitions that, when coupled with parasitic elements (leakage inductances, junction capacitances), result in a stiff ODE system exhibiting widely separated time constants [13]. Stiff systems of this nature require implicit numerical integration to maintain computational stability across disparate temporal scales without resorting to excessively small time steps [14, 15].

To optimize the balance between computational cost and numerical accuracy, several implicit ODE solvers were benchmarked under identical simulation conditions: 0.07 s physical time with relative tolerance set to 10^{-3}. Performance metrics included wall-clock execution time and solution accuracy assessed through waveform comparison. The evaluation compared `ode23tb` (a second-order TR-BDF2 method) against `ode23s` (a modified Rosenbrock formula of order 2) [16].

Our benchmarking revealed that switching from `ode23tb` to `ode23s` reduced simulation time by 88.9% (from approximately three hours to 20 minutes per 70 ms run). While minor waveform shape variations were observed, quantitative feature agreement remained above 95% across all monitored signals, ensuring that degradation signatures were preserved. These gains directly addressed the scalability challenge, enabling the production of the complete 26-level degradation dataset within a practical timeframe. Consequently, `ode23s` was adopted for all subsequent simulations.

3.2. Stage 2: Controlled Fault Injection

With the model configured for efficient simulation, component degradation was introduced through controlled parametric fault injection. Following the degradation model defined in Equation 1, the scaling factor k was swept across 26 discrete levels from $k = 1.00$ to $k = 1.25$ in increments of 0.01, with each simulation run corresponding to one degradation level.

This discrete formulation gives two practical advantages for machine-learning-oriented degradation characterization. First, because k remains constant within each run, the electrical signals stabilize rapidly, enabling short simulations sufficient to capture the steady-state signature at each state. Second, each simulation output is unambiguously labeled by its degradation factor k, producing structured datasets directly suitable for supervised learning.

The 26-run sweep was executed in batch, capturing 13 sensor signals per run and generating 364 output files in total (26 simulations $\times$ 13 signals, plus label files). All MOSFETs in the converter (four primary-side and six secondary-side) are degraded uniformly by the same factor k, establishing a symmetric reference scenario. In real operation, switching position and load profile produce non-uniform stress across devices: primary-side switches experience different thermal and electrical loading than secondary-side MOSFETs, which leads to differential aging rates.

The uniform assumption adopted here isolates the effect of degradation state on electrical signatures from variability in degradation distribution, providing a controlled baseline for feature characterization. Asymmetric degradation patterns are left for future work.

3.3. Stage 3: Feature Engineering

Raw time-series outputs from Stage 2 were transformed into compact, discriminative indicators suitable for machine learning through feature extraction and ranking.

Preprocessing: The 364 signal files were consolidated into a unified timetable. Our threshold-based settling-time analysis showed that all signals reach 98% of their steady-state values within about 27.5 ms. To ensure robust feature extraction from stable operating conditions, data before 40 ms was removed, retaining only the steady-state period where degradation-induced variations are clearly distinguishable from transient startup dynamics.

Extraction: For each sensor signal, we computed 18 features. The 13 time-domain features included 6 statistical features (Mean, Root Mean Square (RMS), Standard Deviation, Shape Factor, Kurtosis, Skewness), 4 impulsive features (Crest Factor, Impulse Factor, Clearance Factor, Peak Value), and 3 harmonic features (Signal-to-Noise Ratio (SNR), Total Harmonic Distortion (THD), Signal-to-Noise and Distortion (SINAD)). The 5 frequency-domain features comprised 2 spectral peaks (Peak Amplitude, Peak Frequency), 2 model coefficients (Natural Frequency, Damping Factor), and 1 band power measure. This yielded 234 candidate condition indicators across the 13 instrumented channels.

Ranking: We used two complementary algorithms to rank features by importance. Monotonicity (Spearman's ρ, scored 0–1) assessed the consistency of each feature's trend with increasing k: scores approaching 1 indicate a reliable increase or decrease across all degradation levels, a desirable property for prognostic applications. One-way ANOVA quantified between-group variance through the F-statistic, identifying features that best separate different degradation levels. For each degradation level, the steady-state window (40–70 ms) was partitioned into 10 non-overlapping segments of 3 ms each, providing 10 replicate feature values per k-level and ensuring that the F-test has sufficient within-group degrees of freedom.

3.4. Stage 4: Prognostic Model Development

In the simulation environment, k is a known input parameter. The regression model trained on this data learns the mapping from observable electrical measurements to degradation state, yielding a state-level diagnostic estimator. Once trained, this mapping is intended for use on real hardware, where the

actual degradation level is unobservable: the model would take sensor measurements as input and provide an estimate $\hat{k}$ of the current degradation state. This diagnostic estimate is also the input the prognostic chain consumes once a temporal degradation law $k(t)$ is available. The simulation thus serves to generate the labeled training data needed to learn the mapping that becomes operational at deployment.

The five top-ranked features identified in Stage 3 constitute the input vector for regression models that map observable electrical signatures to degradation factor k. Because k is a continuous variable encoding $R_{\mathrm{DS(on)}}$ drift severity, regression preserves the ordinal progression of degradation and supports interpolation between discrete simulation points.

Training protocol: We trained regression models using an 80/20 train-test split with 5-fold cross-validation across the 26-sample dataset. We systematically trained and compared 26 regression algorithms spanning linear models, tree-based methods, support vector machines, Gaussian processes, kernel approximation, ensembles, and neural networks. This allowed us to select the best model based on cross-validated performance.

4. RESULTS AND DISCUSSION

Here we present the results, with a focus on feature selection outcomes, model accuracy, and out-of-sample behavior.

4.1. Feature Selection and Degradation Sensitivity

The feature ranking process identified five condition indicators with superior discriminative power across the 26 degradation levels, combining monotonicity analysis and one-way ANOVA variance testing. Table 2 summarizes the top-ranked features and their performance metrics.

Table 2. Top-Ranked Prognostic Features

Feature	Monotonicity	ANOVA F-stat.
Mean(I_{HV1})	0.999	209
RMS(I_{HV1})	0.280	163
THD(V_{LV1})	0.551	457
Shape Factor(V_{LV1})	0.326	858
SINAD(V_{LV1})	0.152	575

Note: I_{HV1} = High-voltage circuit input current; V_{LV1} = Voltage after transformer.

Among the 234 candidate features, Mean(I_{HV1}) achieved near-perfect monotonicity (0.999), exhibiting a consistent upward trend with increasing degradation factor k, as shown in Fig. 2. This makes physical sense: as $R_{\mathrm{DS(on)}}$ increases, conduction losses go up, and the closed-loop voltage regulation compensates by pulling more input current to keep the 28 V output.

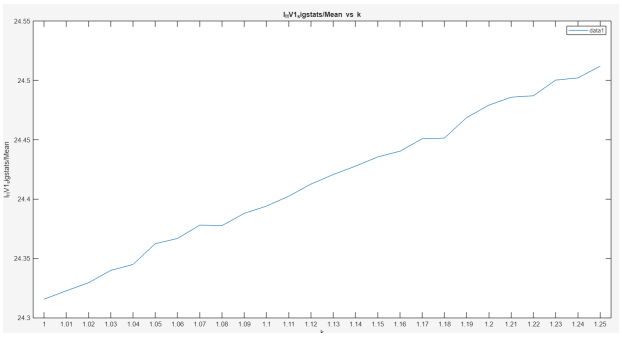

Figure 2. Mean(I_{HV1}) vs. degradation factor k.

While the remaining four features show lower monotonicity scores, they were selected for their high ANOVA F-statistics, indicating strong discriminative power between different degradation levels. Shape Factor(V_{LV1}) achieved the highest F-statistic (858), suggesting it captures subtle changes in waveform morphology that effectively separate degradation states despite not following a strictly monotonic trend.

The top features predominantly originated from high-voltage input current (I_{HV1}) and low-voltage output voltage (V_{LV1}) measurements. Current-based features captured the increased power demand under degradation, while voltage-based harmonic and shape metrics (THD, SINAD, Shape Factor) reflected distortions in output waveform quality as switch resistance increased.

4.2. Regression Model Performance

Among the 26 regression models systematically trained and evaluated, Linear Regression achieved the best performance with a cross-validated RMSE of 0.003758. Table 3 compares representative models from each algorithm family.

Table 3. Regression Model Performance Comparison

Model Type	RMSE
Linear Regression	0.003758
Robust Linear	0.003777
Stepwise Linear	0.003809
Quadratic SVM	0.005090
Linear SVM	0.005261
Medium Gaussian SVM	0.005937
Fine Tree	0.008183
Medium Tree	0.01376
Coarse Tree	0.03563

The three linear model variants (Linear, Robust Linear, and Stepwise Linear) performed nearly identically, with RMSE values all clustering around 0.0038 and $R^2 > 0.99$. This consistency confirms that the relationship between the selected features and degradation factor k is approximately linear. More complex models, including Support Vector Machines with nonlinear kernels and tree-based methods, showed progressively worse performance, with the Coarse

Tree achieving RMSE of 0.03563, nearly ten times higher than the linear models.

The fitted linear regression equation is:

$$\begin{aligned}\hat{k} = 32.734 &+ 0.397\,\mathrm{Mean}(I_{\mathrm{HV1}}) - 0.288\,\mathrm{RMS}(I_{\mathrm{HV1}}) \\ &- 5.442\,\mathrm{SINAD}(V_{\mathrm{LV1}}) - 15.864\,\mathrm{SF}(V_{\mathrm{LV1}}) \\ &- 10.881\,\mathrm{THD}(V_{\mathrm{LV1}})\end{aligned} \tag{2}$$

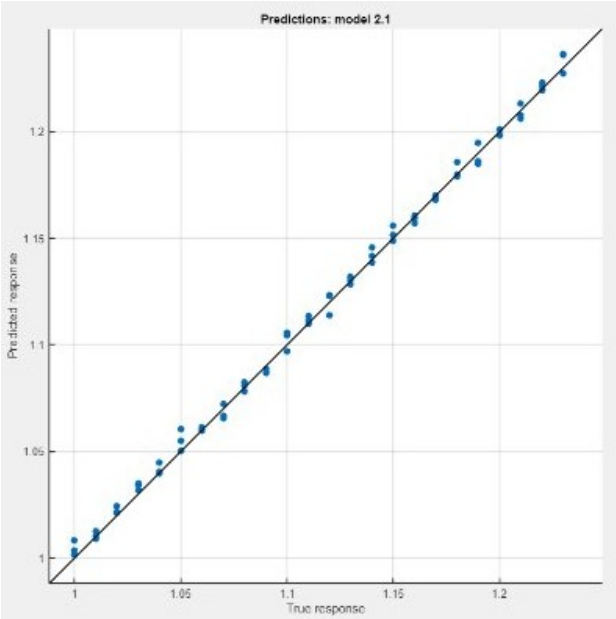

Figure 3. Predicted vs. actual degradation factor k.

Figure 3 shows the predicted versus actual degradation factor for all 26 samples, demonstrating the model's ability to accurately estimate k across the full range from nominal ($k = 1.00$) to end-of-life ($k = 1.25$) conditions.

Because several of the selected features are derived from the same physical signals, the individual regression coefficients in Equation 2 should be interpreted collectively rather than as isolated feature contributions; the mapping as a whole, not any single coefficient, carries the diagnostic information.

To verify the model's behavior outside the training grid, predictions were evaluated on seven additional simulations spanning intermediate degradation levels within the training range and one extrapolation point beyond the end-of-life threshold ($k = 1.30$). The linear regression model maintained absolute errors below 0.007 across all seven points, confirming that the learned mapping remains stable both between adjacent training values and modestly beyond them.

5. CONCLUSION

This work addressed a fundamental challenge in developing Prognostics and Health Management capabilities for aerospace power converters during the design phase: the lack of degradation data needed to train and validate prognostic algorithms. This work repurposes an existing control-oriented electrical model for PHM development, demonstrating that component degradation can be estimated even though the model does not explicitly capture multi-physics degradation processes.

When applied to a 10 kW aeronautical DC/DC converter with SiC MOSFET degradation as the target failure mode, the approach successfully generated labeled degradation datasets using optimized simulation, identified the electrical signals and features carrying the most prognostic information about MOSFET degradation through combined monotonicity and ANOVA ranking, and trained regression models achieving high accuracy (RMSE = 0.0038, $R^2 > 0.99$). The resulting linear model provides a real-time diagnostic estimator of the degradation factor k from observable electrical signatures, which the prognostic chain consumes once a temporal degradation law $k(t)$ is available.

Three simplifying assumptions bound the present scope. First, all MOSFETs are degraded uniformly by the same factor k, whereas real devices experience non-uniform stress across switching positions. Second, as set out in Section 2.3, the simulation runs at a fixed operating temperature, so the reversible thermal component of $R_{\mathrm{DS(on)}}$ is held constant rather than modeled. Recovering the aging-only signal on real hardware, where junction temperature varies with load and ambient conditions, will require thermal compensation or a concurrent temperature measurement, which falls outside the present scope. Third, the simulation produces noise-free signals, whereas real measurements include sensor noise and other measurement imperfections that the trained estimator has not seen.

Even within these bounds, this work delivers one of the two components a complete RUL pipeline requires: a diagnostic estimator $\hat{k}$ that infers the current degradation state from electrical measurements, and a temporal degradation law $k(t)$, generally stochastic in nature, mapping degradation state to operating time. This work develops the diagnostic component, demonstrating that $\hat{k}$ can be learned from design-stage simulation data and accurately estimated for unseen degradation levels. The second component, $k(t)$, depends on the operating profile and thermal history of the device and must be derived from accelerated life test data currently being acquired through the Aeroconverter project. Once both components are available, the RUL at operating time t is obtained by computing the mean time remaining until the device reaches the end-of-life threshold $k_{\mathrm{EoL}} = 1.25$.

Ongoing work within the Aeroconverter project addresses four further directions: updating model parameters based on functional test data from physical prototypes to improve fidelity; integrating coupled thermo-electrical simulation to capture temperature-resistance feedback and thermal cycling effects; characterizing the estimator's robustness to measurement noise and sensor uncertainty before deployment on real hardware; and implementing the degradation trajectories under varying operational profiles, including non-uniform degradation across switching positions, to support prescriptive maintenance strategies that optimize component replacement timing and minimize unscheduled removals in operational aircraft [17].

By demonstrating what is achievable with existing design tools, this work establishes clear priorities for where to invest in experimental validation and advanced modeling efforts.

REFERENCES

[1] S. Kumar, B. Allard, M. Hologne-Carpentier, G. Clerc, and F. Auger, "Review of prognosis approaches applied to power SiC MOSFETs for health state and remaining useful life prediction," *Entropy*, 2026.

[2] J. R. Celaya, A. Saxena, P. Wysocki, S. Saha, and K. Goebel, "Towards prognostics of power MOSFETs: Accelerated aging and precursors of failure," *Annual Conference of the PHM Society*, 2010.

[3] W. Wu, Y. Gu, M. Yu, C. Gao, and Y. Chen, "Remaining useful lifetime prediction based on extended Kalman particle filter for power SiC MOSFETs," *Micromachines*, 2023.

[4] N. B. Hölzel, T. Schilling, and S. Langhans, "Aircraft lifecycle cost-benefit analysis of PHM systems," *Annual Conference of the PHM Society*, n.d.

[5] G. Akbar, A. D. Fatta, G. Rizzo, G. Ala, P. Romano, and A. Imburgia, "Comprehensive review of wide-bandgap (WBG) devices: SiC MOSFET and its failure modes affecting reliability," *Physchem*, vol. 5, no. 1, p. 10, 2025.

[6] H. Huang and P. A. Mawby, "A lifetime estimation technique for voltage source inverters," *IEEE Transactions on Power Electronics*, vol. 29, no. 8, pp. 4113–4119, 2014.

[7] N. Patil, J. Celaya, D. Das, K. Goebel, and M. Pecht, "Precursor parameter identification for insulated gate bipolar transistor (IGBT) prognostics," *IEEE Transactions on Reliability*, vol. 58, no. 2, pp. 271–276, 2009.

[8] J. W. Sheppard, M. A. Kaufman, and T. J. Wilmering, "IEEE standards for prognostics and health management," *Aerospace Conference*, n.d.

[9] *Design Assurance Guidance for Airborne Electronic Hardware*, RTCA, Inc. Std. DO-254, 2000.

[10] *Simscape Electrical – Specialized Power Systems*, MathWorks, 2024. [Online]. Available: https://www.mathworks.com/help/sps/specialized-power-systems.html

[11] P. S. Kathribail and T. Vijayakumar, "Comprehensive study of MOSFET degradation in power converters and prognostic failure detection using physical model," *Journal of The Institution of Engineers (India): Series B*, 2023.

[12] J. Harikumaran, G. Buticchi, G. Migliazza, and M. Galea, "Failure modes and reliability oriented system design for aerospace power electronic converters," *IEEE Open Journal of the Industrial Electronics Society*, 2021.

[13] S. A. M. Yatim, Z. B. Ibrahim, K. I. Othman, and M. B. Suleiman, "A quantitative comparison of numerical methods for solving stiff ordinary differential equations," *Mathematical Problems in Engineering*, vol. 2011, p. 193691, 2011.

[14] C. W. Gear, *Numerical Initial Value Problems in Ordinary Differential Equations*. Englewood Cliffs, NJ: Prentice-Hall, 1971.

[15] G. D. Byrne and A. C. Hindmarsh, "Stiff ODE solvers: A review of current and coming attractions," *Journal of Computational Physics*, vol. 70, no. 1, pp. 1–62, 1987.

[16] The MathWorks, Inc., *MATLAB Documentation: Ordinary Differential Equation Solvers*, The MathWorks, Inc., Natick, MA, 2024. [Online]. Available: https://www.mathworks.com/help/matlab/math/choose-an-ode-solver.html

[17] N. Esposito, L. Saintis, B. Castanier, S. Verron, and M. Giorgio, "A Prescriptive Maintenance Policy for Degrading Units in a Civil Aircraft Context," in *35th European Safety and Reliability Conference (ESREL 2025) and the 33rd Society for Risk Analysis Europe Conference (SRA-E 2025)*. Stavanger (Norway): Research Publishing Services, 2025, pp. 1578–1585.